DOI 10.1007/s10891-019-02083-6

Journal of Engineering Physics and Thermophysics, Vol. 92, No. 6, November, 2019

MHD FLOW OF A WILLIAMSON FLUID OVER AN INFINITE ROTATING DISK WITH ANISOTROPIC SLIP

Najeeb Alam Khan[a] and Faqiha Sultan[b]

UDC 532.5

An MHD flow of a Williamson fluid over an infinite rotating disk with the Soret and Dufour effects and an anisotropic slip was investigated. The system of nonlinear partial differential equations governing this flow and the heat and mass transfer in it was rearranged to the ordinary differential equations with the use of the von Kármán similarity transformation. The ordinary differential equations were numerically solved using the MATLAB routine bvp4c.

Keywords: *Williamson fluid, rotating disk, anisotropic slip, Soret–Dufour effects.*

Introduction. Recently major attention has been concentrated on the analysis of non-Newtonian fluids because of their numerous applications in industry and engineering. The most common example of the non-Newtonian fluids are the pseudoplastic ones. Pseudoplastic fluids are used in the preparation of emulsion sheets, such as photographic films, in the extrusion of polymer sheets, in the formation of plasma and blood flows, and in other processes. The rheological properties of such fluids cannot be defined with the use of only the Navier–Stokes equations. To overcome this deficiency, several rheological models, such as the Carreau model, power-law model, Ellis model, and Cross model, have been developed. In 1929, Williamson [1] presented a detailed description of pseudoplastic materials, proposed a constitutive equation that defines the flow characteristics of pseudoplastic fluids, and experimentally validated the results obtained. The correspondence of this model of a non-Newtonian fluid to blood flow has attracted the attention of researchers. Many valuable works have been added to this field in recent years. Nadeem et al. [2] presented a study on the two-dimensional flow of a Williamson fluid over a stretched sheet. Khan et al. [3] investigated the effect of a chemical reaction on the boundary layer flow of a Williamson fluid. Zehra et al. [4] proposed a numerical solution of the problem on the Williamson fluid flow with a pressure-dependent viscosity over an inclined channel. Malik et al. [5] presented the solution of the problem on the homogeneous and heterogeneous reactions in a Williamson fluid over a stretched cylinder with the use of a Keller box. Recently, Malik et al. [6] performed a numerical investigation on the influence of the variable thermal conductivity of a Williamson fluid and the generation/absorption of heat by it on its flow and the heat transfer in it.

An exact solution of the momentum equations governing the steady flow generated by an infinite disk rotating with a uniform angular velocity was proposed for the first time by Kármán [7]. It was assumed that in the direction of the flow close to the disk there are no pressure gradients that would balance the centrifugal forces so that the fluid would spiral outward. The disk works as a centrifugal fan: the flow generated by it is supplemented by an axial flow retracing to the surface of the disk. The problem on the flow of a Newtonian fluid over a rotating disk has attracted considerable attention from researchers. The problem on the flow of a non-Newtonian fluid over a rotating disk has received much less attention despite the fact that this flow has found many applications in engineering. Some of the recent works were devoted to the study of the effect of a magnetic field on the laminar flow of a non-Newtonian Eyring–Powell fluid over a rotating disk [8], the stability of the boundary layer of the flow of a non-Newtonian fluid over a rotating disk [9], and the effect of double diffusion on the unsteady MHD flow of a couple-stress fluid over a rotating disk and the heat transfer in it [10].

The latest developments in micro- and nanotechnology made it possible to use micro- and nanosized devices in many applications. In such devices, the surface properties play a major role. Lately the hydrophobic and hydrophilic

[a]Department of Mathematics, University of Karachi, Karachi, 75270, Pakistan; email: njbalam@yahoo.com; [b]Department of Mathematics, NED University of Engineering & Technology, Karachi, 75270, Pakistan. Published in Inzhenerno-Fizicheskii Zhurnal, Vol. 92, No. 6, pp. 2674–2685, November–December, 2019. Original article submitted May 15, 2017.

surfaces obtained with the use of micro- and nanotechnologies have attracted much attention. It was established that the drag of a flow in a microsized channel is decreased due to the slip of this flow on the hydrophobic surface of the channel. Recently, superhydrophobic surfaces have attracted much attention because they make it possible to substantially decrease the skin-friction drag in turbulent flows. Several engineering applications of these surfaces have been explored lately [11–13]. The flows over some surfaces show an evident slip denying the traditional no-slip condition. In 1823, Navier [14] proposed a slip boundary condition, in accordance with which the slip velocity of a flow depends linearly on the shear stress in it. In recent years, some advances have been achieved in the study of flows over such surfaces. Ng and Wang [11] investigated the emploiment of superhydrophobic surfaces and investigated the Stokes shear flow over a grating. Later, they obtained two- and three-dimensional patterns of the slip of the Stokes flow over a surface with the use of the semianalytical technique [15]. Busse and Sandham [16] investigated the influence of the anisotropic Navier slip-length boundary condition on the turbulent flow in a channel. Wang [17] investigated the axisymmetric stagnation flow over a moving plate with different streamwise and spanwise slip coefficients. Recently, Cooper et al. [18] have presented a theoretical study on the effect of anisotropic and isotropic slips on the stability of the boundary layer flow over a rotating disk.

Many technical and industrial applications, such as the cooling of electronic devices by fans, nuclear reactors during emergency shutdowns, and heat exchangers with low-velocity flows, are based on forced and free convection. In such devices, a cross-diffusion also takes place due to the simultaneous occurrence, in them, of heat transfer and mass transfer that influence each other. The mass transfer affected by a temperature gradient is known as the Soret effect, whereas the heat transfer affected by a concentration gradient is known as the Dufour effect. Osalusi et al. [19] investigated the Dufour and Soret effects in a steady convective flow, generated by a rotating disk, with heat and mass transfer, Ohmic heating, and viscous dissipation under slip conditions in the presence of a magnetic field. Shatei and Motsa [20] investigated the boundary layer flow over an unsteady stretching surface with a Hall-current and a Soret–Dufour effects. Narayana and Sibanda [21] investigated the effect of a double diffusive on a flow over a cone. Recently, Khan and Sultan [22] have presented the flow of an Eyring–Powell fluid over a cone bounded by a porous medium with Soret and Dufour effects.

A survey of literature has shown that the structure of the flow of a Williamson fluid over a rotating disk, the Soret and Dufour effects in it, the influence of an anisotropic slip on this flow, and its heat and mass transfer characteristics have not been analyzed so far, despite the fact that the indicated parameters of such a flow are of importance when is used in oceanography, rotating machinery, nanotechnology, electronic and nuclear devices, and computer storage devices, and control of these parameters of a flow makes it possible to decrease the skin-friction drag in it. In the present work, an effort has been made to overcome this deficiency and investigate the influence of an anisotropic slip of a MHD flow over a rotating disk with Soret and Dufour effects on the structure of this flow and the heat and mass transfer in it. The von Kármán similarity transformation was used to transform the ordinary differential equations governing the momentum and the heat and mass transfer characteristics of the indicated flow to the partial differential equations. The model of this flow, including all the above effects, is very complex and, therefore, it cannot be solved analytically. A numerical solution of this model was obtained with the use of the MATLAB routine bvp4c.

Mathematical Model. A pseudoplastic fluid following the Williamson rheological model is considered. The tensor of an extra stress in a Williamson fluid is defined as

$$\tau = (\mu_\infty + (\mu_0 - \mu_\infty)(1 - \Gamma\dot{\gamma})^{-1})A\,, \tag{1}$$

where Γ is the time constant, $A = \nabla V + (\nabla V)^t$ is the strain-rate tensor, ∇ is the differential operator, and

$$\dot{\gamma} = \sqrt{\frac{1}{2}\,trA^2}\,. \tag{2}$$

Using the first-order Taylor series approximation of $(1 - \Gamma\dot{\gamma})^{-1} \cong (1 + \Gamma\dot{\gamma})$ with $\Gamma^2 <<< 1$, we bring Eq. (1) to the form

$$\tau = (\mu_0 + (\mu_0 - \mu_\infty)\Gamma\dot{\gamma})A\,. \tag{3}$$

The shear components of a Williamson fluid in cylindrical polar coordinates have the form

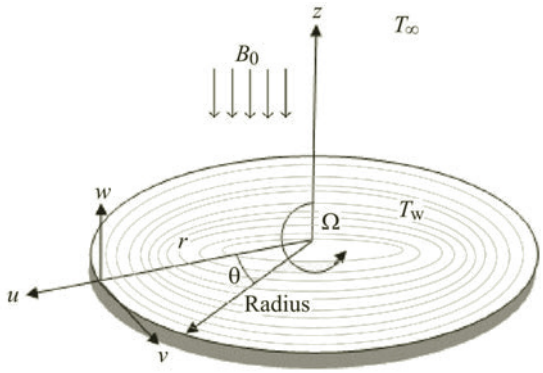

Fig. 1. Physical model of the fluid flow and coordinate system.

$$\tau_{rr} = 2(\mu_0 + (\mu_0 - \mu_\infty)\Gamma\dot{\gamma})\left(\frac{\partial u}{\partial r}\right), \quad \tau_{r\theta} = \tau_{\theta r} = (\mu_0 + (\mu_0 - \mu_\infty)\Gamma\dot{\gamma})\left(\frac{1}{r}\frac{\partial u}{\partial \theta} + \frac{\partial v}{\partial r} - \frac{v}{r}\right),$$

$$\tau_{\theta\theta} = 2(\mu_0 + (\mu_0 - \mu_\infty)\Gamma\dot{\gamma})\left(\frac{1}{r}\frac{\partial v}{\partial \theta} + \frac{u}{r}\right), \quad \tau_{rz} = \tau_{zr} = (\mu_0 + (\mu_0 - \mu_\infty)\Gamma\dot{\gamma})\left(\frac{\partial u}{\partial z} + \frac{\partial w}{\partial r}\right), \tag{4}$$

$$\tau_{zz} = 2(\mu_0 + (\mu_0 - \mu_\infty)\Gamma\dot{\gamma})\left(\frac{\partial w}{\partial z}\right), \quad \tau_{\theta z} = \tau_{z\theta} = (\mu_0 + (\mu_0 - \mu_\infty)\Gamma\dot{\gamma})\left(\frac{1}{r}\frac{\partial w}{\partial \theta} + \frac{\partial v}{\partial z}\right),$$

$$\dot{\gamma} = \sqrt{2\left(\frac{\partial u}{\partial r}\right)^2 + \left(\frac{\partial v}{\partial r} + \frac{1}{r}\frac{\partial u}{\partial \theta} - \frac{v}{r}\right)^2 + \left(\frac{\partial u}{\partial z} + \frac{\partial w}{\partial r}\right)^2 + 2\left(\frac{1}{r}\frac{\partial v}{\partial \theta} + \frac{u}{r}\right)^2 + \left(\frac{1}{r}\frac{\partial w}{\partial \theta} + \frac{\partial v}{\partial z}\right)^2 + 2\left(\frac{\partial w}{\partial z}\right)^2}. \tag{5}$$

Formulation of the Problem. We consider a steady three-dimensional, axisymmetric incompressible flow of a Williamson fluid over a rotating disk with heat and mass transfer. This flow is produced by an infinite hydrophobic disk rotating with a constant angular velocity Ω. The fluid propagates infinitely in the positive half-space of the disk ($z > 0$), and it is initially located at $z = 0$. The disk has different slips in the radial and tangential directions. A uniform external magnetic field of strength B_0 is applied normally to the disk. The schematic diagram of the problem is presented in Fig. 1. The temperature at the surface of the disk T_w and the species concentration at this surface C_w remain unchanged. The temperature T_∞ and concentration C_∞ of the ambient fluid are uniform at a constant pressure P_∞.

Assuming that the above-described fluid flow has a small Reynolds number, we write the following system of equations for this flow and the heat and mass transfer in it:

$$\frac{\partial u}{\partial r} + \frac{u}{r} + \frac{\partial w}{\partial z} = 0\,, \tag{6}$$

$$\rho\left(u\frac{\partial u}{\partial r} - \frac{v^2}{r} + w\frac{\partial u}{\partial z}\right) = -\frac{\partial p}{\partial r} + \frac{\partial \tau_{rr}}{\partial r} + \frac{\partial \tau_{zr}}{\partial z} + \frac{\tau_{rr} - \tau_{\theta\theta}}{r} - \sigma B_0^2 u\,, \tag{7}$$

$$\rho\left(u\frac{\partial v}{\partial r} + \frac{uv}{r} + w\frac{\partial v}{\partial z}\right) = \frac{\partial \tau_{r\theta}}{\partial r} + \frac{\partial \tau_{z\theta}}{\partial z} + 2\frac{\tau_{r\theta}}{r} - \sigma B_0^2 v\,, \tag{8}$$

$$\rho\left(u\frac{\partial w}{\partial r} + w\frac{\partial w}{\partial z}\right) = -\frac{\partial p}{\partial z} + \frac{\partial \tau_{rz}}{\partial r} + \frac{\partial \tau_{zz}}{\partial z} + \frac{\tau_{rz}}{r}\,, \tag{9}$$

$$u\frac{\partial T}{\partial r} + w\frac{\partial T}{\partial z} = \frac{k}{\rho C_P}\left(\frac{\partial^2 T}{\partial r^2} + \frac{1}{r}\frac{\partial T}{\partial r} + \frac{\partial^2 T}{\partial z^2}\right) + \frac{D_m K_T}{C_s C_P}\left(\frac{\partial^2 C}{\partial r^2} + \frac{1}{r}\frac{\partial C}{\partial r} + \frac{\partial^2 C}{\partial z^2}\right), \tag{10}$$

$$u\,\frac{\partial C}{\partial r} + w\,\frac{\partial C}{\partial z} = D\left(\frac{\partial^2 C}{\partial r^2} + \frac{1}{r}\,\frac{\partial C}{\partial r} + \frac{\partial^2 C}{\partial z^2}\right) + \frac{D_{\mathrm{m}} K_T}{T_{\mathrm{av}}}\left(\frac{\partial^2 T}{\partial r^2} + \frac{1}{r}\,\frac{\partial T}{\partial r} + \frac{\partial^2 T}{\partial z^2}\right), \tag{11}$$

with the boundary conditions

$$\begin{gathered} u = k_1 \tau_{rz}\,, \quad v = r\Omega + k_2\ \tau_{\theta\, z}\,, \quad w = 0\,, \quad P = 0\,, \quad T = T_{\mathrm{w}}\,, \quad C = C_{\mathrm{w}}\,, \quad \text{at} \quad z = 0\,, \\ u \to 0\,, \quad v \to 0\,, \quad w \to 0\,, \quad T \to T_\infty\,, \quad C \to C_\infty \quad \text{as} \quad z \to \infty\,. \end{gathered} \tag{12}$$

Similarity transformation. To obtain the dimensionless continuity, momentum, energy, and concentration equations for the fluid flow being considered, we use the similarity solution of the Navier–Stokes equations, obtained by Kármán [7]:

$$\begin{gathered} f(\eta) = \frac{u}{r\Omega}\,, \quad g(\eta) = \frac{v}{r\Omega}\,, \quad h(\eta) = \frac{w}{\sqrt{\nu\Omega}}\,, \quad P(\eta) = \frac{p}{\rho\nu\Omega}\,, \quad \Theta(\eta) = \frac{T - T_\infty}{T_{\mathrm{w}} - T_\infty}\,, \\ \varphi(\eta) = \frac{C - C_\infty}{C_w - C_\infty}\,, \quad \eta = \sqrt{\frac{\Omega}{\nu}}\,z\,, \quad \mathrm{Re} = \frac{\Omega r^2}{\nu}\,. \end{gathered} \tag{13}$$

Using the above similarity transformation, we represent Eqs. (6)–(11) in the form

$$2f + h' = 0\,, \tag{14}$$

$$\begin{gathered} (1 + \mathrm{We}\dot\gamma) f'' - f^2 + g^2 - h f' - Mf + \frac{\mathrm{WeRe}}{\dot\gamma^3}\,(f'' f'^2 + f' g' g'') \\ + \frac{2\mathrm{We}}{\dot\gamma^3}\,(3 f f'^2 + f g'^2 + f' h' h'') = 0\,, \end{gathered} \tag{15}$$

$$(1 + \mathrm{We}\dot\gamma) g'' - h g' - 2 f g - Mg + \frac{\mathrm{WeRe}}{\dot\gamma^3}\ (f' g' f'' + g'^2 g'') + \frac{2\mathrm{We}}{\dot\gamma^3}\,(2 f f' g' + g' h' h'') = 0\,, \tag{16}$$

$$\begin{gathered} P' + h\,h' - 2(1 + \mathrm{We}\dot\gamma)(f' + h'') \\ - \frac{\mathrm{WeRe}}{\dot\gamma^3}\,(f'^3 + f' g'^2 + f' h' f'' + h' g' g'') - \frac{4\mathrm{We}}{\dot\gamma^3}\,(2 f f' h' + h'^2 h'') = 0\,, \end{gathered} \tag{17}$$

$$\Theta'' - \mathrm{Pr}\ h\Theta' + \mathrm{Df}\ \varphi'' = 0\,, \tag{18}$$

$$\varphi'' - \mathrm{Sh}\ \varphi' + \mathrm{Sr}\ \Theta'' = 0\,, \tag{19}$$

where

$$\dot\gamma = \sqrt{4 f^2 + \mathrm{Re}(f'^2 + g'^2) + 2h'^2}\,, \quad \mathrm{We} = \frac{\Omega\Gamma(\mu_0 - \mu_\infty)}{\mu_0}, \quad M = \frac{\sigma B_0^2}{\rho\Omega}\,, \quad \mathrm{Pr} = \frac{\mu_0 C_P}{k}\,,$$

$$\mathrm{Df} = = \frac{\rho D K_T}{k C_{\mathrm{s}}}\,\frac{C_{\mathrm{w}} - C_\infty}{T_{\mathrm{w}} - T_\infty}\,, \ \text{and} \quad \mathrm{Sr} = \frac{D_{\mathrm{m}} K_T}{D T_{\mathrm{av}}}\,\frac{T_{\mathrm{w}} - T_\infty}{C_{\mathrm{w}} - C_\infty}.$$

The boundary conditions (12) are transformed as

$$f(0) = \lambda_1 f'(0)\left(1 + \mathrm{We}\sqrt{4(f(0))^2 + \mathrm{Re}((f'(0))^2 + (g'(0))^2) + 2(h'(0))^2}\right),$$

$$g(0) = 1 + \lambda_2 g'(0)\left(1 + \mathrm{We}\sqrt{4(f(0))^2 + \mathrm{Re}((f'(0))^2 + (g'(0))^2) + 2(h'(0))^2}\right),$$

$$h(0) = 0\,, \quad P(0) = 0\,, \quad \Theta(0) = 1\,, \quad \varphi(0) = 1\,, \tag{20}$$

$$f(\infty) = 0\,, \quad g(\infty) = 0\,, \quad \Theta(\infty) = 0\,, \quad \varphi(\infty) = 0\,,$$

where $\lambda_1 = k_1\mu_0\sqrt{\dfrac{\Omega}{\nu}}$ and $\lambda_2 = k_2\mu_0\sqrt{\dfrac{\Omega}{\nu}}$.

Physical parameters. The shear stress coefficients, the moment of friction, and the local Nusselt and Sherwood numbers of a von Kármán flow with heat and mass transfer are important physical parameters. The coefficients of radial and tangential shear stresses in the Williamson fluid at the surface of the disk are defined as

$$(C_f, C_g) = \left(\frac{\tau_{rz}}{\mu_0\Omega}, \frac{\tau_{\theta z}}{\mu_0\Omega}\right)\Bigg|_{z=0}. \tag{21}$$

Hence, we have the following relations for the local skin-friction coefficients:

$$\frac{C_f}{\sqrt{\mathrm{Re}}} = \left(1 + \mathrm{We}\sqrt{4(f(0))^2 + \mathrm{Re}((f'(0))^2 + (g'(0))^2) + 2(h'(0))^2}\right) f'(0)\,, \tag{22}$$

$$\frac{C_g}{\sqrt{\mathrm{Re}}} = \left(1 + \mathrm{We}\sqrt{4(f(0))^2 + \mathrm{Re}((f'(0))^2 + (g'(0))^2) + 2(h'(0))^2}\right) g'(0)\,. \tag{23}$$

Another interesting parameter of a fluid flow over a rotating disk is the turning moment of the disk with fluid on both its sides, known as the moment of friction. This parameter is determined from the tangential velocity profile by integrating the shear stresses of the fluid over the disk surface. The moment coefficient C_m for the Williamson fluid over a rotating disk is determined from the expression

$$C_m = \frac{-2\pi}{\sqrt{\mathrm{Re}}}\left(1 + \mathrm{We}\sqrt{4f^2 + \mathrm{Re}(f'^2 + g'^2) + 2h'^2}\right) g'\,. \tag{24}$$

The heat and mass flows at the surface of the rotating disk are fefined as

$$(q_\mathrm{w}, M_\mathrm{w}) = \left(-k\left(\frac{\partial T}{\partial z}\right), -D\left(\frac{\partial C}{\partial z}\right)\right)\Bigg|_{z=0}. \tag{25}$$

Hence, for the Nusselt and Sherwood numbers, we have the expression

$$(\mathrm{Nu}, \mathrm{Sh}) = -\sqrt{\mathrm{Re}}(\Theta'(0), \varphi'(0))\,. \tag{26}$$

Numerical Method. The momentum and heat and mass transfer properties of a Williamson fluid over a rotating disk with Soret and Dufour effects have not been studied yet because of the complexity of the system of governing equations. This system is highly nonlinear, and it consists of coupled ordinary differential equations that are quite difficult to solve analytically. Moreover, the presence of slip terms in the boundary conditions additionally complicates the indicated system. To overcome these difficulties, the system was numerically solved using the MATLAB routine based on the numerical bvp4c method offered by Kierzenka and Shampine [23]. Many engineering problems were successfully solved by this method.

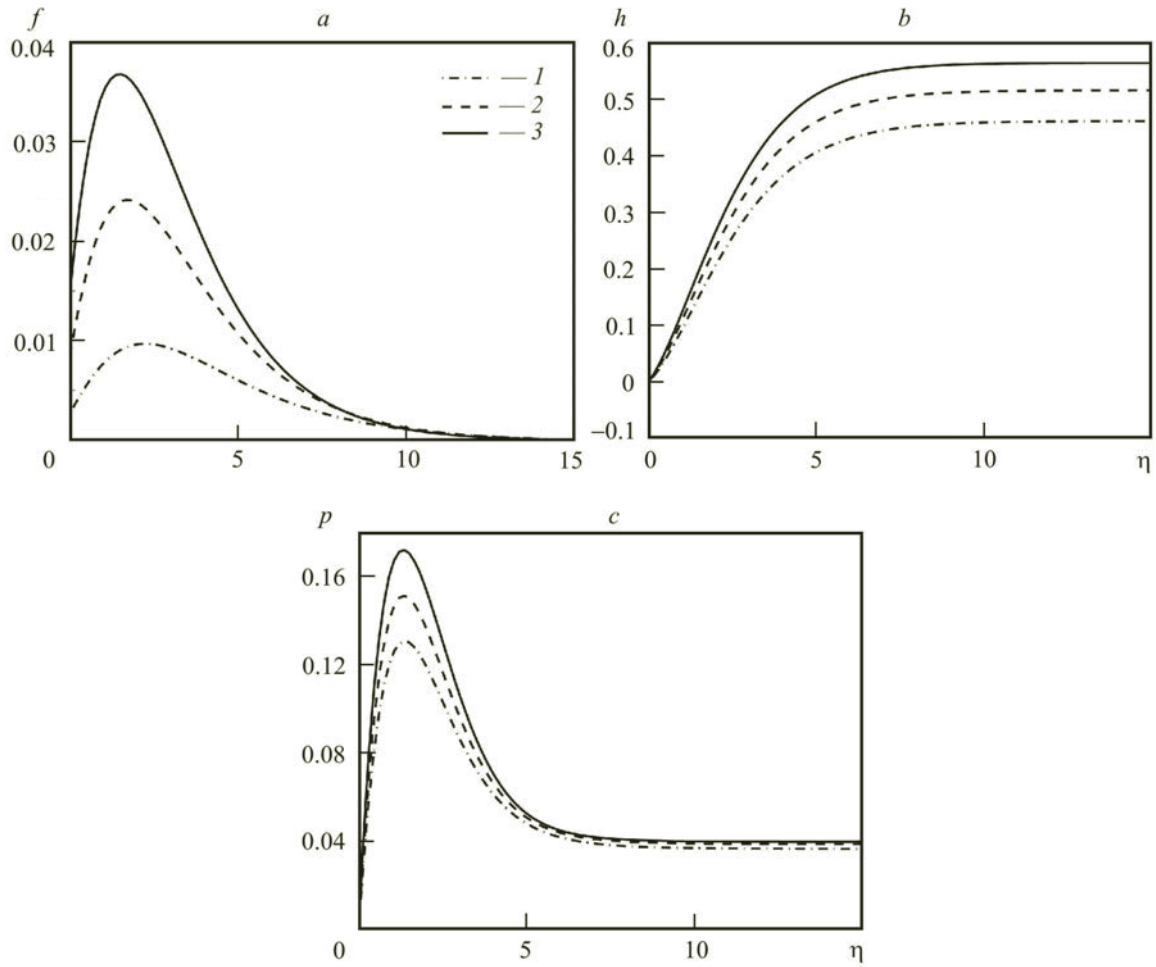

Fig. 2. Distributions of the radial (a) and axial (b) velocities of the fluid flow and of the pressure in it (c) under the anisotropic slip conditions at We = 0.4 (1), 0.6 (2), and 0.8 (3).

Results and Discussion. The anisotropic slip of the fluid flow of a Williamson fluid generated by a rotating infinite disk as well as the Soret and Dufour effects and the heat and mass transfer in it were determined from the numerical solution of the system of governing equations for this flow. Results of investigations of the influence of the indicated parameters of the fluid flow on its velocity, pressure, temperature, and concentration distributions are presented in Figs. 2–10. The validity of the model proposed and the results obtained with it was proved by comparison of the numerical data obtained for a special case of Williamson fluid where We = 0 (Tables 1 and 2). The numerical values of some important physical parameters of a Williamson fluid are presented in Tables 3 and 4. For simplicity, constant values were taken for some parameters: We = 0.4, $\lambda_1 = 0.4$, $\lambda_2 = 0.2$, M = 0.1, $M = 0.1$, Re = 0.1, Df = 0.5, Sr = 0.2, Sh = 1.0, and Pr = 6.

The general structure of the profiles of the radial, tangential, and axial velocities of the fluid flow, observed from the figures, can be theoretically described in the following way: the radial velocity profile shows the rapid growth near the disk, and then it steadily diminishes to zero, allowing more fluid to pass through the disk; the tangential velocity profile appears to be exponentially decaying, and the axial velocity profile takes a limiting asymptotic value. The effects of the Williamson parameter on the velocity profiles of the fluid flow and the pressure distribution in it are presented in Fig. 2. It is seen from Fig. 2a that the Williamson parameter has increasing impact on the radial velocity of the flow near the disk, which allows a larger amount of the fluid to pass through the disk, but it shows no effect as the velocity profile moves away from the disk. At the same time, as seen from Fig. 2b, the Williamson parameter has increasing influence on the axial velocity away from the disk. It is seen from Fig. 2c that the pressure distribution also increases with increase in We. The influence of the radial slip on the radial and axial velocities of the fluid flow in the presence of a tangential slip is presented in Fig. 3a and b: the impact is quite similar to the effect of the Williamson parameter. The radial slip increases the radial and

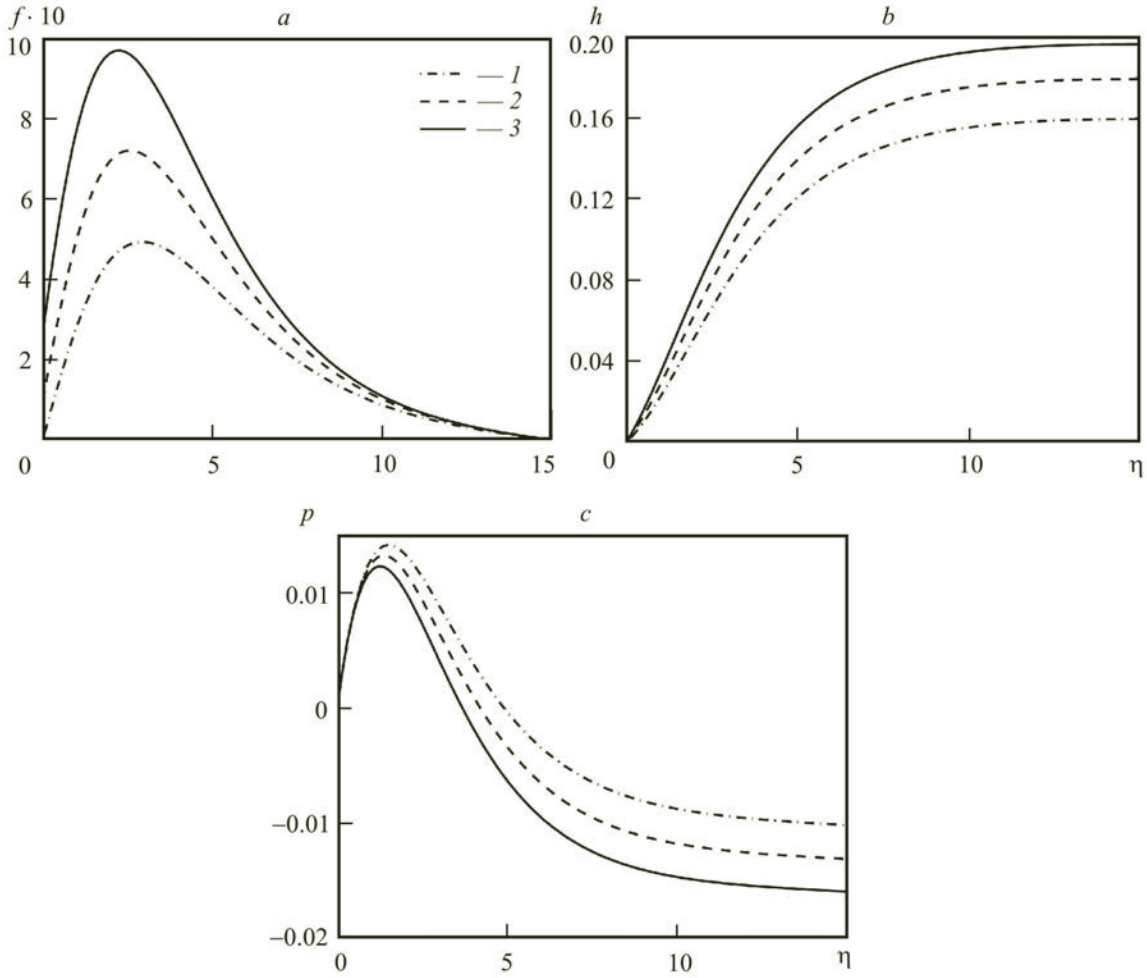

Fig. 3. Distributions of the radial (a) and axial (b) velocities of the fluid flow and of the pressure in it (c) under the tangential slip conditions at $\lambda_1 = 0$ (1), 0.2 (2), and 0.4 (3).

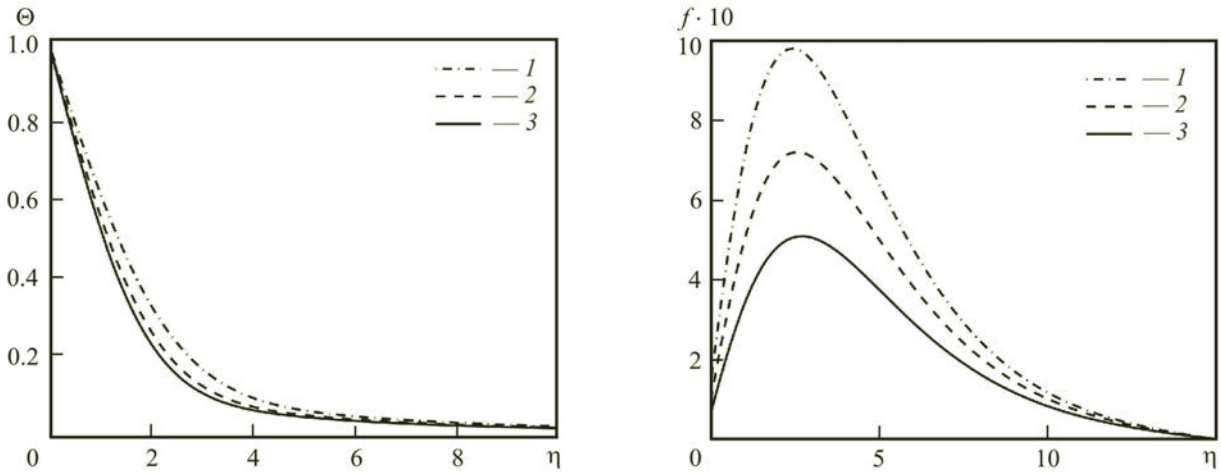

Fig. 4. Temperature distribution in the fluid flow with a tangential slip at $\lambda_1 = 0$ (1), 1 (2), and 2 (3).

Fig. 5. Distribution of the radial velocity of the fluid flow with a radial slip at $\lambda_2 = 0$ (1), 0.2 (2), and 0.4 (3).

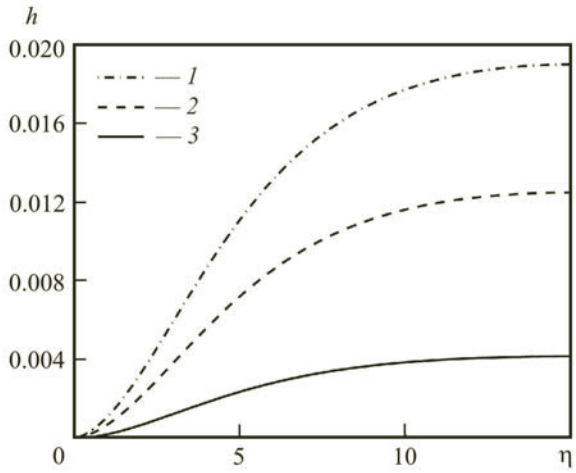

Fig. 6. Distributions of the axial velocity of the fluid flow with a radial slip at $\lambda_2 = 0$ (1), 0.04 (2), and 0.08 (3).

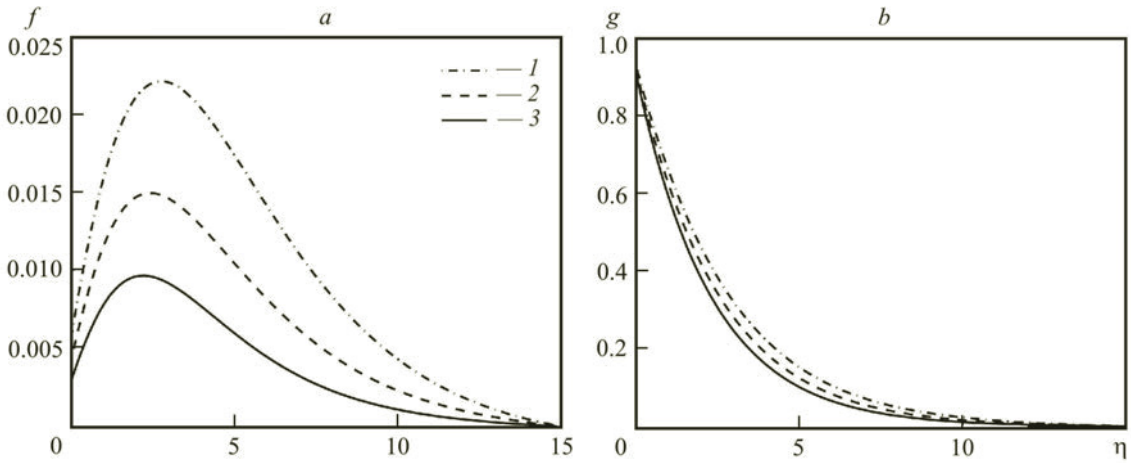

Fig. 7. Distributions of the radial (a) and tangential (b) velocities of the fluid flow with an anisotropic slip at M = 0 (1), 0.05 (2), and 0.1 (3).

TABLE 1. Values of Some Physical Parameters of the Fluid Flow Obtained in the Present Work and in [24] at We = 0, $M = 0$, Pr = 0.71, Sh = 0.6, Df = 0, and Sr = 0

Physical quantities	Present work	[24]
$f'(0)$	0.5102	0.51023
$-g'(0)$	0.6159	0.61592
$-h(\infty)$	0.8844	0.8838
$-P(\infty)$	0.3911	0.3906

axial flow velocities. However, as seen from Fig. 3c and Fig. 4, the pressure and temperature profiles decrease when the radial slip increases. On the other hand, as is seen from Figs. 5 and 6, an increase in the tangential slip substantially reduces the radial and axial velocities. Figure 7 shows the influence of the magnetic field on the radial and tangential velocities of the flow, and both profiles show a decreasing behavior with increase in magnetic field. The influence of the temperature and

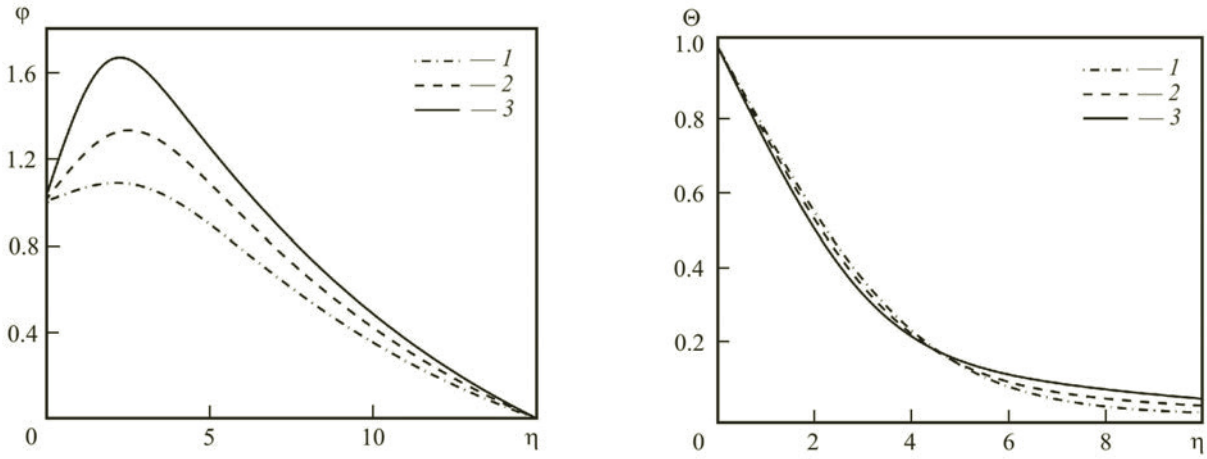

Fig. 8. Concentration distribution in the fluid flow with an anisotropic slip at Sr = 0 (1), 0.4 (2), and 0.8 (3).

Fig. 9. Temperature distribution in the fluid flow with an anisotropic slip at Df = 0 (1), 0.4 (2), and 0.8 (3).

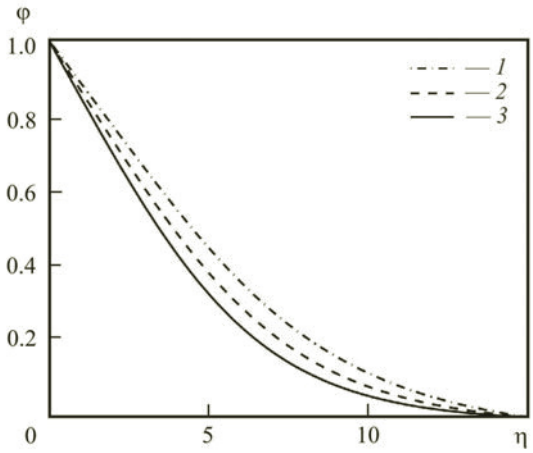

Fig. 10. Concentration distribution in the fluid flow with an anisotropic slip at Sc = 0.2 (1), 0.8 (2), and 1.4 (3).

TABLE 2. Dependences of the Temperature of the Fluid Flow on the Prandtl Number Obtained in the Present Work and in [25] at We = 0, M = 0, Sh = 0.6, Df = 0, and Sr = 0

Pr	$-\Theta'(0)$	
	Present work	[25]
0.71	0.3286	0.32857
1	0.3962	0.39626
10	1.1341	1.1341
100	2.6871	2.8672

TABLE 3. Values of the Local Skin Friction Coefficients C_f and C_g and the Moment of Friction C_m Depending on We, λ_1, λ_2, and M at Re = 0.1, Df = 0.5, Sr = 0.2, Sc = 1.0, and Pr = 6

We	λ_1	λ_2	M	$\mathrm{Re}^{-\frac{1}{2}} C_f$	$\mathrm{Re}^{-\frac{1}{2}} C_g$	C_m
0.4				0.0066	0.3295	6.5461
0.6	0.4	0.2	0.1	0.0211	0.3758	7.4677
0.8				0.0371	0.4176	8.2980
	0.0			0.0032	0.3126	6.2110
0.4	0.2	0.2	0.1	0.0049	0.3203	6.3633
	0.4			0.0066	0.3295	6.5461
		0.0		0.0092	0.3636	7.2253
0.4	0.4	0.2	0.1	0.0066	0.3295	6.5461
		0.4		0.0047	0.3025	6.0105
			0.0	0.0130	0.2166	4.3032
10	0.2	0.2	0.05	0.0097	0.2758	5.4791
			0.1	0.0066	0.3295	6.5461

TABLE 4. Values of the Local Nusselt and Sherwood Numbers Depending on We, λ_1, λ_2, M, Pr, Df, and Sr at Re = 0.1

We	λ_1	λ_2	M	Pr	Df	Sr	$\mathrm{Re}^{-\frac{1}{2}}$ Nu	$\mathrm{Re}^{-\frac{1}{2}}$ Sh
0.4							0.2319	0.0686
0.6	0.4	0.2	0.1	6	0.5	0.2	0.3692	0.0924
0.8							0.4603	0.1148
	0.0						0.1571	0.0651
0.4	0.2	0.2	0.1	6	0.5	0.2	0.1944	0.0663
	0.4						0.2319	0.0686
		0.0					0.2664	0.0732
0.4	0.4	0.2	0.1	6	0.5	0.2	0.2319	0.0686
		0.4					0.2009	0.0659
			0.0				0.3291	0.0988
0.4	0.4	0.2	0.05	6	0.5	0.2	0.2823	0.0809
			0.1				0.2319	0.0686
				1			0.0851	0.0965
0.4	0.4	0.2	0.1	3	0.5	0.2	0.1555	0.0829
				5			0.2096	0.0728
					0.0		0.2346	0.0681
			0.1		0.5	0.2	0.2319	0.0686
					1.0		0.2288	0.0693
						0.0	0.2212	0.1003
0.4	0.4	0.2	0.1	6	0.5	0.5	0.2319	0.0686
						1.0	0.2442	0.0324

diffusion effects on the mass transfer in the fluid flow is demonstrated in Fig. 8. It is clearly seen that an increase in the Soret number increases the mass transfer in the fluid flow. Figure 9 shows the behavior of the temperature profile of the fluid vs the Dufour number. The temperature distribution decreases near the disk, and its pattern changes away from the disk. The influence of the Schmidt number on the concentration profile of the fluid flow is presented in Fig. 10. It is seen from this figure that the concentration profile decreases with increase in the Schmidt number.

A Williamson fluid shows viscous behavior at We = 0 and $\mu_0 \to \mu_\infty$ or $\Gamma = 0$. Considering this property of the Williamson fluid, the model of flow of a Williamson fluid over a rotating disk with an anisotropic slip and the results obtained with it were verified by comparison of them with the results obtained in [24] for viscous fluid flows over a rotating disk (Table 1). In Table 2, the numerical data on the heat transfer in the fluid flow at different values of the Prandtl number are compared with the corresponding results obtained in [25]. The numerical comparisons presented in both tables prove the validity of the model developed. The numerical values of the radial and tangential skin-friction coefficients and the coefficient of friction are presented in Table 3, and the numerical values of the local Nusselt number and the local Sherwood number are given in Table 4. In follows from Table 3 that the Williamson parameter exerts similar effects on the skin-friction drag in both the radial and tangential directions and on the moment of friction: all the quantities increase with increase in We. The effects of the radial slip on the radial and tangential skin-friction drags are opposite in character to those of the tangential slip. The radial slip increases the skin-friction in both directions with increase in the moment of friction, while the tangential slip decreases both the skin-friction coefficients and the moment of friction. However, the skin-friction in the radial direction decreases with increase in the magnetic field, but it increases the drag in the tangential direction with increase in the moment of friction. Moreover, as seen from Table 4, an increase in We increases the heat and mass transfer in the fluid, and the radial slip increases the local Nusselt and Sherwood numbers, but the tangential slip and the magnetic field decrease these quantities. On the other hand, the Prandtl, Dufour, and Soret numbers differently influence the Nusselt and Sherwood numbers. The Prandtl and Soret numbers increase the heat transfer and decrease the mass transfer in the fluid flow, but the Dufour number decreases the heat transfer and increases the mass transfer in this flow.

Conclusions. A numerical investigation of the Soret and Dufour effects on the MHD flow of a Williamson fluid over an infinite rotating disk with an anisotropic slip has been performed. It was established that an anisotropic slip and the Soret and Dufour effects significantly influence the structure of the indicated flow and the heat and mass transfer in it. Radial slip increases the radial velocity of the flow, and tangential slip decreases the flow velocity in this direction. A magnetic field decreases both the radial and azimuthal velocities of the flow. The adequacy of the numerical data obtained was confirmed by comparison of them with the analogous data found in the literature.

NOTATION

B_0, magnetic field; C, species concentration in the boundary layer; C_P, specific heat at a constant pressure; C_s, concentration susceptibility; C_w, species concentration at the wall; C_∞, species concentration in the ambient fluid; D, molecular diffusivity; f, h, and g, radial, axial, and tangential components of the dimensionless flow velocity; Df, Pr Re, and Sr, Dufour, Prandtl, Reynolds, and Soret numbers; D_m, effective mass-flow diffusivity; k, thermal conductivity; k_1 and k_2, radial and tangential slip coefficients; K_T, thermal-diffusion ratio; M, magnetic field parameter; Nu and Sh, local Nusselt and Sherwood numbers; p, hydrostatic pressure; P_∞, constant pressure; P, dimensionless dynamic pressure in the fluid above the disk; T and T_{av}, temperature and average temperature of the fluid, K; T_w, temperature of the disk wall, K; T_∞, free-stream temperature, K; u, v, and w, fluid-velocity components in the x, y, and z directions; V, velocity of the fluid flow; We, Williamson parameter; $\dot{\gamma}$, second invariant of the strain-rate tensor; η, dimensionless distance from the surface of the disk; Θ and φ, dimensionless temperature and concentration of the fluid; λ_1 and λ_2, radial and tangential slip parameters; μ_0 and μ_∞, zero and infinite viscosity shear rates; $\nu = \dfrac{\mu_0}{\rho}$, kinematic viscosity; ρ, density of the fluid; τ, extra stress tensor. Subscripts: av, average; m, mass; s, susceptibility; w, wall.

REFERENCES

1. R. V. Williamson, The flow of pseudoplastic materials, *Ind. Eng. Chem*., **21**, 1108–1111 (1929).
2. S. Nadeem, S. T. Hussain, and C. Lee, Flow of a Williamson fluid over a stretching sheet, *Braz. J. Chem. Eng*., **30**, 619–625 (2013).
3. N. A. Khan, S. Khan, and F. Riaz, Boundary layer flow of Williamson fluid with chemically reactive species using scaling transformation and homotopy analysis method, *Math. Sci. Lett.*, **3**, 199–205 (2014).

4. I. Zehra, M. M. Yousaf, and S. Nadeem, Numerical solutions of Williamson fluid with pressure dependent viscosity, *Results Phys*., **5**, 20–25 (2015).
5. M. Y. Malik, T. Salahuddin, A. Hussain, S. Bilal, and M. Awais, Homogeneous-heterogeneous reactions in Williamson fluid model over a stretching cylinder by using Keller box method, *AIP Adv.*, **5**, 107227 (2015).
6. M. Y. Malik, M. Bibi, F. Khan, and T. Salahuddin, Numerical solution of Williamson fluid flow past a stretching cylinder and heat transfer with variable thermal conductivity and heat generation/absorption, *AIP Adv.*, **6**, 035101 (2016).
7. T. V. Kármán, Über laminare und turbulente Reibung, *J. Appl. Math. Mech.*, **1**, 233–252 (1921).
8. N. A. Khan, S. Aziz, and N. A. Khan, MHD flow of Powell–Eyring fluid over a rotating disk, *J. Taiwan Inst. Chem. Eng*., **45**, 2859–2867 (2014).
9. P. T. Griffiths, S. O. Stephen, A. P. Bassom, and S. J. Garrett, Stability of the boundary layer on a rotating disk for power-law fluids, *J. Non-Newtonian Fluid* Mech., **207**, 1–6 (2014).
10. N. A. Khan, S. Aziz, and N. A. Khan, Numerical simulation for the unsteady MHD flow and heat transfer of couple stress fluid over a rotating disk, *PLoS One*, **9**, e95423 (2014).
11. C.-O. Ng and C. Y. Wang, Stokes shear flow over a grating: Implications for superhydrophobic slip, *Phys. Fluids*, **21**, 013602:013601-013612 (2009).
12. H. Park, H. Park, and J. Kim, A numerical study of the effects of superhydrophobic surface on skin-friction drag in turbulent channel flow, *Phys. Fluids*, **25**, 110815: 110811–110811 (2013).
13. J. P. Rothstein, Slip on superhydrophobic surfaces, *Ann. Rev. Fluid Mech*., **42**, 89–109 (2010).
14. C. Navier, Mémoire sur les lois du mouvement des fluides, *Mem. Acad. R. Sci. Inst. France*, **6**, 389–440 (1823).
15. C.-O. Ng and C. Y. Wang, Effective slip for Stokes flow over a surface patterned with two- or three-dimensional protrusions, *Fluid Dyn. Res*., **43**, 065504 (2011).
16. A. Busse and N. D. Sandham, Influence of an anisotropic slip-length boundary condition on turbulent channel flow, *Phys. Fluids*, **24**, 055111 (2012).
17. C. Y. Wang, Stagnation flow on a plate with anisotropic slip, *Eur. J. Mech.-B/Fluids*, **38**, 73–77 (2013).
18. A. J. Cooper, J. H. Harris, S. J. Garrett, M. Özkan, and P. J. Thomas, The effect of anisotropic and isotropic roughness on the convective stability of the rotating disk boundary layer, *Phys. Fluids*, **27**, 014107 (2015).
19. E. Osalusi, J. Side, R. Harris, and P. Clark, The effect of combined viscous dissipation and Joule heating on unsteady mixed convection MHD flow on a rotating cone in a rotating fluid with variable properties in the presence of Hall and ion-slip currents, *Int. Commun. Heat Mass Transf*., **35**, 413–429 (2008).
20. S. Shateyi and S. S. Motsa, Boundary layer flow and double diffusion over an unsteady stretching surface with Hall effect, *Chem. Eng. Commun*., **198**, 1545–1565 (2011).
21. M. Narayana and P. Sibanda, On the solution of double-diffusive convective flow due to a cone by a linearization method, *J. Appl. Math*. Article ID 587357 (2012).
22. N. A. Khan and F. Sultan, On the double diffusive convection flow of Eyring–Powell fluid due to cone through a porous medium with Soret and Dufour effects, *AIP Adv.*, **5**, 057140 (2015).
23. J. Kierzenka and L. F. Shampine, A BVP solver based on residual control and the Maltab PSE, *ACM Trans. Math. Software*, **27**, 299–316 (2001).
24. F. M. White, *Viscous Fluid Flow*, 2nd edn., McGraw-Hill, Singapore (1991).
25. H.-T. Lin and L.-K. Lin, Heat transfer from a rotating cone or disk to fluids of any Prandtl number, *Int. Commun. Heat Mass Transf*., **14**, 323–332 (1987).